LETTER

doi:10.1038/nature26144

Timing of oceans on Mars from shoreline deformation

Robert I. Citron[1,2], Michael Manga[1,2] & Douglas J. Hemingway[1,2]

Widespread evidence points to the existence of an ancient Martian ocean[1–8]. Most compelling are the putative ancient shorelines in the northern plains[2,7]. However, these shorelines fail to follow an equipotential surface, and this has been used to challenge the notion that they formed via an early ocean[9] and hence to question the existence of such an ocean. The shorelines' deviation from a constant elevation can be explained by true polar wander occurring after the formation of Tharsis[10], a volcanic province that dominates the gravity and topography of Mars. However, surface loading from the oceans can drive polar wander only if Tharsis formed far from the equator[10], and most evidence indicates that Tharsis formed near the equator[11–15], meaning that there is no current explanation for the shorelines' deviation from an equipotential that is consistent with our geophysical understanding of Mars. Here we show that variations in shoreline topography can be explained by deformation caused by the emplacement of Tharsis. We find that the shorelines must have formed before and during the emplacement of Tharsis, instead of afterwards, as previously assumed. Our results imply that oceans on Mars formed early, concurrent with the valley networks[15], and point to a close relationship between the evolution of oceans on Mars and the initiation and decline of Tharsis volcanism, with broad implications for the geology, hydrological cycle and climate of early Mars.

Distinct geological boundaries (contacts) lining the northern plains of Mars for thousands of kilometres have been interpreted as palaeo-shorelines and evidence of an early ocean[2–4,6,7]. However, observed long-wavelength deviations (by up to several kilometres) in shoreline elevation from an equipotential have been used as an argument against the emplacement of the contacts by a body of liquid water, the interpretation of the features as shorelines, and the existence of a Martian ocean[9]. Perron *et al.*[10] showed that the elevation changes of two extensive contacts, Arabia (contact 1) and Deuteronilus (contact 2), can be explained by deformation due to 30°–60° and 5°–25° of post-Tharsis true polar wander (TPW), respectively, because a varying rotation pole also changes the orientation of a planet's equatorial bulge, or polar flattening, altering equipotential surfaces (such as sea levels) globally. Such large magnitudes of TPW can be driven by ocean loading/unloading, but only if Tharsis formed far from the equator[10]. If Tharsis formed near the equator, then the remnant fossil bulge would have prevented ocean loading from causing large amounts of post-Tharsis TPW (see Extended Data Fig. 1).

Most evidence points to the formation of Tharsis near the equator[11–15]. Mars' remnant rotational figure (fossil bulge) is close to the equator, indicating a palaeopole of (259.5 ± 49.5° E, $71.1^{+17.5}_{-14.4}$° N), the likely pre-Tharsis orientation of Mars[14]. The pre-Tharsis palaeopole also matches the likely orientation of Mars during valley network formation[15]. Formation of Tharsis probably drove only limited (approximately 20°) TPW to reach Mars' current configuration, which precludes the possibility that surface loads drove sufficient TPW to deform the shorelines[10,16].

We propose that the Arabia shoreline instead formed before or during the early stages of Tharsis emplacement, which initiated > 3.7 billion years (Gyr) ago[17] when the rotation pole of Mars was at the palaeopole (259.5° E, 71.1° N) corresponding to the fossil bulge[14]. The Arabia shoreline, potentially emplaced at least 4 Gyr ago[6], would have been modified by both topographic changes from Tharsis (which dominates Mars' topography and gravity on a global scale; see Extended Data Fig. 2), and the approximately 20° of Tharsis-induced TPW. The Deuteronilus shoreline, which differs less from a present-day equipotential than the older Arabia shoreline, is dated to about 3.6 Gyr ago[18], after most of Tharsis was emplaced. However, Tharsis had complex and multi-stage growth that extended into the Hesperian and Amazonian[17,19], meaning that the Deuteronilus shoreline would have been deformed by the late stages of Tharsis' emplacement. We examine a chronology in which shoreline deformation is due mainly to Tharsis (Table 1), and compare expected deformation due to Tharsis with the elevation profiles of the Arabia and Deuteronilus contacts.

Assuming the Arabia shoreline formed before Tharsis, and the Deuteronilus shoreline formed after most of Tharsis was emplaced, we compare the best fits for the deformation expected from Tharsis to the current topography of the shorelines, including an offset factor Z to represent sea level at the time of shoreline formation. We also examine the Isidis shoreline, which formed 100 million years (Myr) after Deuteronilus[18]. For the Arabia shoreline emplaced before Tharsis, deformation is expressed as the contribution of Tharsis to Mars' topography along the shoreline, and the change in topography from limited Tharsis-induced TPW. For the Deuteronilus and Isidis shorelines emplaced during the late stages of Tharsis growth, deformation is taken as the percentage of Tharsis' contribution to topography occurring after the shorelines formed, and no contribution from TPW (because reorientation should occur within tens of thousands of years to a few million years after the Tharsis plume reaches the surface[20], much less than the 100 Myr or more that lies between Tharsis initiation and Deuteronilus formation). See Methods for more details.

We show that the Arabia shoreline's deviations from an equipotential can be explained almost entirely by deformation due to Tharsis emplacement (Fig. 1). Our best fit (equation (3) with $Z = -2.3$ km) yields a root-mean square misfit σ_{rms} of 0.615 km, comparable to the error values from Perron *et al.*[10], and follows the slope of the shoreline data better from 1,000 km to 6,600 km. The limited Tharsis-induced TPW has a negligible effect. A slightly lower σ_{rms} is obtained if only 80% of Tharsis topography was emplaced after the Arabia shoreline formed (Extended Data Fig. 3). However, the difference between the fits using 80% or 100% of Tharsis' topography is negligible considering the scatter in the shoreline data. Our model therefore suggests that the Arabia shoreline formed before or during the early stages of Tharsis' growth.

The Deuteronilus shoreline's deviations from an equipotential can be explained by deformation due to the emplacement of about 17% of Tharsis topography (Fig. 2), indicating that the shoreline formed during the late stages of Tharsis' growth. Our best fit (equation (4) with

[1]Department of Earth and Planetary Science, University of California, Berkeley, Berkeley, California, USA. [2]Center for Integrative Planetary Science, University of California, Berkeley, Berkeley, California, USA.

Table 1 | Possible evolution of Martian shorelines

Time (epoch)	Event	Effect
At least 4 Gyr ago (Early Noachian)	Arabia shoreline forms	
>3.6 Gyr ago (Late Noachian/Early Hesperian)	Majority of Tharsis forms	Both Tharsis emplacement/loading and Tharsis-induced TPW (20°) deform the Arabia shoreline
3.6 Gyr ago (Early Hesperian)	Deuteronilus shoreline forms	
3.5 Gyr ago (Late Hesperian)	Isidis shoreline forms	
3.6 Gyr ago to present (Early Hesperian–Late Amazonian)	Remainder of Tharsis forms	Remaining Tharsis growth deforms the Arabia, Deuteronilus and Isidis shorelines
3.5–3.0 Gyr ago (Late Hesperian/Early Amazonian)	Loading of Utopia basin	Loading of the Utopia basin tilts the Isidis basin and deforms sections of the Deuteronilus shoreline

The table outlines the sequence of events required to produce a pre- or early-Tharsis Arabia shoreline, and the formation of the Deuteronilus shoreline concurrent with the later stages of Tharsis' growth. Explaining the Isidis shoreline's topography requires subsequent loading of the Utopia basin (see Extended Data Fig. 4 and Methods).

$C = 0.17$ and $Z = -3.68$ km) yields $\sigma_{rms} = 0.110$ km. Our fit successfully recovers the low elevation of the Phlegra contact, and also captures the decrease in elevation across Utopia and Elysium West. Neither our model nor the Perron *et al.*[10] model captures the full elevation increase of the Tantalus segment, which may result from the topographic bulge from nearby Alba Patera[18]. For the Isidis shoreline, subsequent loading of the Utopia basin is also required to explain the shoreline's topography (see Extended Data Fig. 4 and Methods).

The relation between the shorelines and global deformation due to Tharsis and its associated TPW is illustrated in Fig. 3a–c (also see Extended Data Fig. 2). We estimate the volume of water that filled the northern plains to the Deuteronilus and Arabia shorelines by subtracting the relevant Tharsis and TPW contributions from Mars' topography (0.25° per pixel gridded MOLA data[21]) and filling the lowlands to shoreline elevation (Fig. 3d–f). We estimate a Deuteronilus ocean volume of about 1.2×10^7 km^3, and an Arabia ocean volume of about 4.1×10^7 km^3. These are lower limits because we do not remove excess terrain, such as Elysium, polar deposits, lava/sediment basin deposits, and short-wavelength Tharsis topography (that is, variations in Tharsis topography that occur over short length scales). For the Arabia ocean, use of a map of Mars with excess terrain removed[15] yields an ocean volume of about 5.5×10^7 km^3. The ocean volumes we compute are slightly lower than previous estimates[22] because the Tharsis topography we subtract is negative in much of the area enclosed by the northern ocean basin.

Short-wavelength deviations in shoreline elevation from our model may be due to our assumptions that both lithospheric thickness and the rate of Tharsis emplacement are spatially uniform. Spatial variations in lithospheric thickness[23] would allow for non-uniform responses to phenomena such as TPW[10], plate flexure and dynamic topography from the Tharsis plume[24]. Spatially variable Tharsis emplacement could also affect shoreline modification. Another consideration is ocean loading, but the computed effect on shoreline elevations is small (see Extended Data Fig. 5 and Methods).

Several other short- and long-wavelength processes could have deformed the shorelines in the 3.5 Gyr or more since their emplacement, including dynamic topography from mantle plumes[24], lithospheric deformation[22,25], glacial erosion[26] and plate flexure from loading/unloading. For example, loading of the Utopia basin may have tilted Isidis (see Methods) and deformed sections of the Deuteronilus shoreline[18]. Other loads that post-date shoreline formation include Elysium, the polar deposits, and sections of Tharsis. Such loads

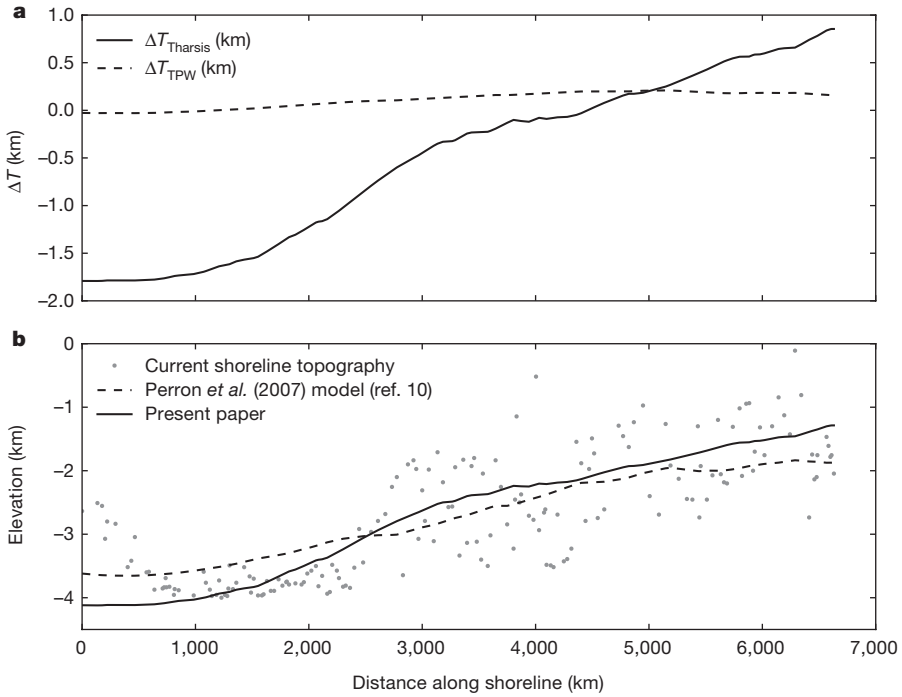

Figure 1 | Comparison of Arabia shoreline topography to shoreline deformation models. a, Change in topography ΔT caused by TPW of 20° (equation (1)) and Tharsis uplift (equation (2)), illustrating that the latter is much more important. **b**, Current topography of the Arabia shoreline from Perron *et al.*[10] (data originally from ref. 7) compared to the Perron *et al.*[10] model of deformation due to post-Tharsis TPW (with $T_e = 200$ km) and our model of deformation due to Tharsis emplacement and induced TPW ($\Delta T_{Tharsis} + \Delta T_{TPW} - 2.3$ km). The starting point for the shoreline is (24.91° W, 13.48° N).

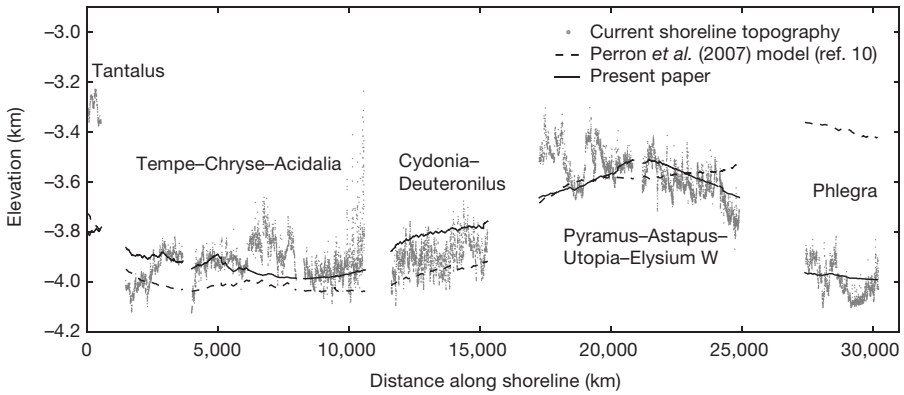

Figure 2 | Comparison of Deuteronilus shoreline topography to shoreline deformation models. Current Deuteronilus topography (data and contact names from ref. 18) compared to the Perron *et al.*[10] model and our model of deformation due to partial Tharsis emplacement ($0.17\Delta T_{\mathrm{Tharsis}} - 3.68$ km). The starting point for the shoreline is (96.40° W, 63.69° N).

could also induce a small amount (<2°) of post-Tharsis TPW[16]. Plate flexure associated with impact basins could also deform shorelines. While basins of over 1,000 km in diameter pre-date the Deuteronilus shoreline, some basins may have been coincident with or post-date the Arabia shoreline. Short-wavelength deformation may also be a consequence of the difficulty in identifying the shorelines themselves[18].

Increased accuracy in shoreline identification and dating[18] can help to reconstruct the history of shoreline formation and modification. Several potential shorelines[6], such as the Ismenius, Acidalia, Elysium, Aeolis and Meridiani contacts, have been relatively unexamined owing to their high degree of discontinuity[7]. Shorelines may also be mismapped; for example, portions of the Meridiani shoreline may be part of the Arabia shoreline[22]. A re-evaluation of shorelines with full consideration of the various deformation processes may enable the development of a chronology of oceans on Mars. In particular, the Meridiani shoreline[6,27] may pre-date the Arabia shoreline and have contained a larger volume of water[22].

Accurate dating of the Arabia shoreline is necessary to determine whether the shoreline formed before or during the early stages of Tharsis' growth. Formation of the Arabia shoreline after some limited early Tharsis growth is suggested by Arabia segments that border Acheron Fossae and Tempe Terra[6], two of the oldest Tharsis units, which are located well north of the expected pre-Tharsis crustal dichotomy boundary (the stark difference in elevation and crustal thickness between the northern lowlands and southern highlands). However, it is possible that the Acheron Fossae and Tempe Terra contacts were misidentified as belonging to the Arabia shoreline, or that the Arabia shoreline initially followed the pre-Tharsis dichotomy boundary, and formed the Tempe Terra and Archaeon Fossae contacts only after early Tharsis uplift and deposition.

The decline in ocean volume from the pre- or early-Tharsis Arabia shoreline to the late-Tharsis Deuteronilus shoreline suggests that Tharsis volcanism may have played a critical part in the evolution of a Martian ocean. After Tharsis was mostly emplaced, by about 3.6 Gyr ago, only short-lived lakes may have been stable[28], although a Late Hesperian/Early Amazonian ocean has also been suggested on the basis of tsunami evidence[8,29]. Outgassing from Tharsis could have contributed to either heating[30] or cooling[31] the planet, both of which could produce the decrease in ocean volume from the Arabia shoreline to the Deuteronilus shoreline as Tharsis activity declined. Either a

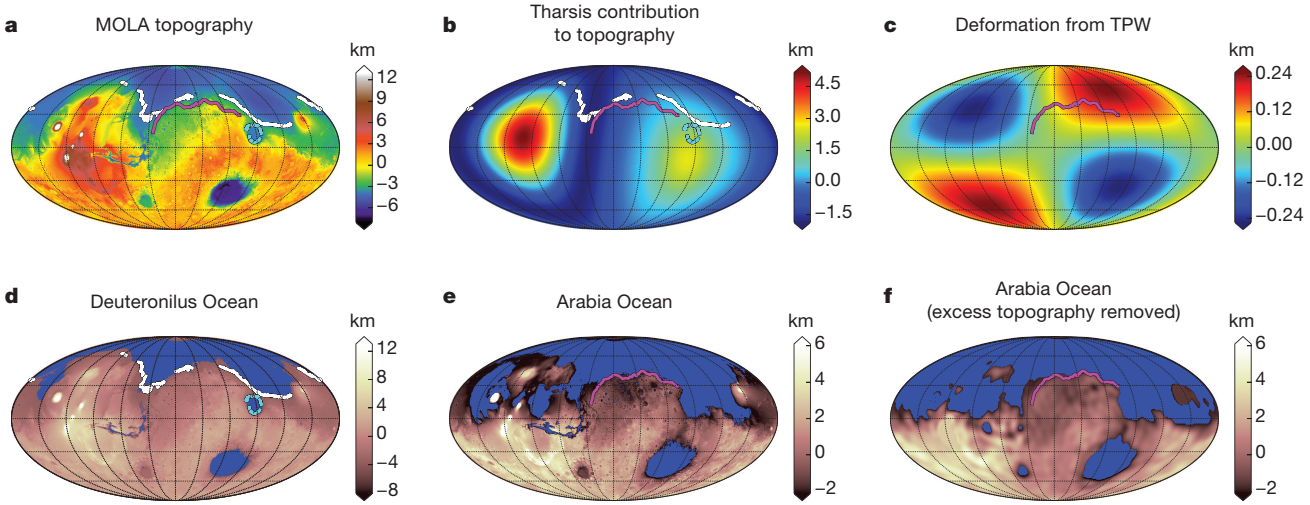

Figure 3 | Shoreline locations relative to current topography, deformation due to Tharsis/TPW, and computed ocean extents. **a**, MOLA topography. **b**, Tharsis contribution to topography (equation (2)). **c**, Deformation due to approximately 20° TPW from the palaeopole corresponding to the fossil bulge[14] with $T_e = 58$ km (equation (1)). **d**, Ocean basin filled to the Deuteronilus shoreline, with the topography of Mars at the time of the Deuteronilus shoreline's formation (MOLA topography minus 17% of Tharsis topography). **e**, Ocean basin filled to the Arabia shoreline, with the topography of Mars at the time of the Arabia shoreline's formation (MOLA topography minus Tharsis topography and deformation due to TPW). Short-wavelength remnants of Tharsis are visible because Tharsis topography is only modelled up to degree-5. **f**, The 'Mars without Tharsis' map[15], which is similar to **e**, but with short-wavelength Tharsis, Elysium, and polar topography removed, filled to the Arabia shoreline. Shorelines are plotted for Deuteronilus (white), Arabia (magenta) and Isidis (cyan), and colour scales denote elevation (or changes in elevation) in kilometres.

large ocean was in place before Tharsis volcanism initiated, and shrank as Tharsis volcanism cooled the planet, or an ocean arose as a result of heating caused by Tharsis outgassing and decreased in volume as Tharsis volcanism declined. It is also possible that each shoreline represents the transient warming of an otherwise frozen ocean or glacial state[30], producing a liquid ocean in periods of heightened Tharsis activity (which, owing to enhanced surface heat flux, may also have resulted in catastrophic circum-Tharsis groundwater discharge[1]). If episodic warming was sufficient to melt most of Mars' glaciers, the decrease in ocean volume may record a declining surface water budget. Although geochemical evidence for a northern ocean is ambiguous[32], an ocean supported by the degassing of sulfur from Tharsis could explain the lack of widespread carbonate deposits observed in the northern plains[33].

The evolution of water on Mars is critical to understanding the past climate and habitability of the planet. Although shorelines on Mars have provided compelling evidence for a Martian ocean, to explain their deviations from an equipotential has been a challenge. We show that the topography of Martian shorelines can be quantitatively explained by deformation due to the emplacement of Tharsis and resulting TPW (in the case of the Arabia shoreline) or by the latter stages of Tharsis emplacement (in the case of the Deuteronilus shoreline). Formation of the Arabia shoreline before (or during the early stages of) Tharsis emplacement suggests that the Arabia ocean was concurrent with valley network incision[15], which probably occurred as part of a globally active hydrosphere capable of supporting such an ocean[5]. The consistency between the topography of the Martian shorelines, their ages, and the chronology of topographic changes due to Tharsis emplacement and associated TPW, suggests that the Arabia and Deuteronilus contacts are evidence that Martian oceans existed, and may have been linked to Tharsis volcanism.

Online Content Methods, along with any additional Extended Data display items and Source Data, are available in the online version of the paper; references unique to these sections appear only in the online paper.

Received 1 October 2017; accepted 25 January 2018.
Published online 19 March 2018.

1. Baker, V. R. *et al.* Ancient oceans, ice sheets and the hydrological cycle on Mars. *Nature* **352,** 589–594 (1991).
2. Parker, T. J., Saunders, R. S. & Schneeberger, D. M. Transitional morphology in West Deuteronilus Mensae, Mars: implications for modification of the lowland/upland boundary. *Icarus* **82,** 111–145 (1989).
3. Parker, T. J., Gorsline, D. S., Saunders, R. S., Pieri, D. C. & Schneeberger, D. M. Coastal geomorphology of the Martian northern plains. *J. Geophys. Res. Planets* **98,** 11061–11078 (1993).
4. Head, J. W. *et al.* Possible ancient oceans on Mars: evidence from Mars Orbiter Laser Altimeter data. *Science* **286,** 2134–2137 (1999).
5. Di Achille, G. & Hynek, B. M. Ancient ocean on Mars supported by global distribution of deltas and valleys. *Nat. Geosci.* **3,** 459–463 (2010).
6. Clifford, S. M. & Parker, T. J. The evolution of the Martian hydrosphere: implications for the fate of a primordial ocean and the current state of the northern plains. *Icarus* **154,** 40–79 (2001).
7. Carr, M. H. & & Head, J. W. Oceans on Mars: an assessment of the observational evidence and possible fate. *J. Geophys. Res. Planets* **108,** 5042 (2003).
8. Rodriguez, J. A. P. *et al.* Tsunami waves extensively resurfaced the shorelines of an early Martian ocean. *Sci. Rep.* **6,** 25106 (2016).
9. Malin, M. C. & Edgett, K. S. Oceans or seas in the Martian northern lowlands: high resolution imaging tests of proposed coastlines. *Geophys. Res. Lett.* **26,** 3049–3052 (1999).
10. Perron, J. T., Mitrovica, J. X., Manga, M., Matsuyama, I. & Richards, M. A. Evidence for an ancient martian ocean in the topography of deformed shorelines. *Nature* **447,** 840–843 (2007).
11. Willemann, R. J. Reorientation of planets with elastic lithospheres. *Icarus* **60,** 701–709 (1984).
12. Roberts, J. H. & Zhong, S. The cause for the north-south orientation of the crustal dichotomy and the equatorial location of Tharsis on Mars. *Icarus* **190,** 24–31 (2007).
13. Daradich, A. *et al.* Equilibrium rotational stability and figure of Mars. *Icarus* **194,** 463–475 (2008).
14. Matsuyama, I. & Manga, M. Mars without the equilibrium rotational figure, Tharsis, and the remnant rotational figure. *J. Geophys. Res. Planets* **115,** E12020 (2010).
15. Bouley, S. *et al.* Late Tharsis formation and implications for early Mars. *Nature* **531,** 344–347 (2016).
16. Kite, E. S., Matsuyama, I., Manga, M., Perron, J. T. & Mitrovica, J. X. True Polar wander driven by late-stage volcanism and the distribution of paleopolar deposits on Mars. *Earth Planet. Sci. Lett.* **280,** 254–267 (2009).
17. Anderson, R. C. *et al.* Primary centers and secondary concentrations of tectonic activity through time in the western hemisphere of Mars. *J. Geophys. Res. Planets* **106,** 20563–20585 (2001).
18. Ivanov, M. A., Erkeling, G., Hiesinger, H., Bernhardt, H. & Reiss, D. Topography of the Deuteronilus contact on Mars: evidence for an ancient water/mud ocean and long-wavelength topographic readjustments. *Planet. Space Sci.* **144,** 49–70 (2017).
19. Dohm, J. M., Baker, V. R., Maruyama, S. & Anderson, R. C. In *Superplumes: Beyond Plate Tectonics* 523–536 (Springer, 2007).
20. Rouby, H., Greff-Lefftz, M. & Besse, J. Rotational bulge and one plume convection pattern: influence on Martian true polar wander. *Earth Planet. Sci. Lett.* **272,** 212–220 (2008).
21. Smith, D. E., Zuber, M. T., Neumann, G. A., Guinness, E. A. & Slaveny, S. Mars Global Surveyor Laser Altimeter mission experiment gridded data record. MGS-M-MOLA-5-MEGDR-L3–V1.0, http://pds-geosciences.wustl.edu/missions/mgs/megdr.html (NASA Planetary Data System, 2003).
22. Ruiz, J., Tejero, R., Gómez-Ortiz, D. & López, V. in *Space Science: New Research* 141–164 (Nova Science, 2006).
23. Grott, M. & Breuer, D. On the spatial variability of the Martian elastic lithosphere thickness: evidence for mantle plumes? *J. Geophys. Res. Planets* **115,** E03005 (2010).
24. Roberts, J. H. & Zhong, S. Plume-induced topography and geoid anomalies and their implications for the Tharsis rise on Mars. *J. Geophys. Res. Planets* **109,** E03009 (2004).
25. Ruiz, J., Fairén, A. G., Dohm, J. M. & Tejero, R. Thermal isostasy and deformation of possible paleoshorelines on Mars. *Planet. Space Sci.* **52,** 1297–1301 (2004).
26. Davila, A. F. *et al.* Evidence for Hesperian glaciation along the Martian dichotomy boundary. *Geology* **41,** 755–758 (2013).
27. Edgett, K. S. & Parker, T. J. Water on early Mars: possible subaqueous sedimentary deposits covering ancient cratered terrain in western Arabia and Sinus Meridiani. *Geophys. Res. Lett.* **24,** 2897 (1997).
28. Kite, E. S. *et al.* Methane bursts as a trigger for intermittent lake-forming climates on post-Noachian Mars. *Nat. Geosci.* **10,** 737–740 (2017).
29. Costard, F. *et al.* Modeling tsunami propagation and the emplacement of thumbprint terrain in an early Mars ocean. *J. Geophys. Res. Planets* **122,** 633–649 (2017).
30. Halevy, I. & Head, J. W. Episodic warming of early Mars by punctuated volcanism. *Nat. Geosci.* **7,** 865–868 (2014).
31. Tian, F. *et al.* Photochemical and climate consequences of sulfur outgassing on early Mars. *Earth Planet. Sci. Lett.* **295,** 412–418 (2010).
32. Pan, L., Ehlmann, B. L., Carter, J. & Ernst, C. M. The stratigraphy and history of Mars' northern lowlands through mineralogy of impact craters: a comprehensive survey. *J. Geophys. Res. Planets* **122,** 1824–1854 (2017).
33. Halevy, I., Zuber, M. T. & Schrag, D. P. A sulfur dioxide climate feedback on early Mars. *Science* **318,** 1903–1907 (2007).

Supplementary Information is available in the online version of the paper.

Acknowledgements We thank J. T. Perron for providing the data for the Arabia shoreline (originally from ref. 7), and M. A. Ivanov for providing the data for the Deuteronilus and Isidis shorelines. We thank I. Matsuyama for discussions regarding this research. R.I.C. and M.M. are supported by NSF EAR-1135382. D.J.H. is supported by the Miller Institute for Basic Research in Science.

Author Contributions All authors discussed the research idea, methods and interpretation of results. R.I.C. and M.M. developed the hypothesis with input from D.J.H. R.I.C. performed the calculations and wrote the manuscript, with guidance, comments, and revisions from M.M. and D.J.H.

Author Information Reprints and permissions information is available at www.nature.com/reprints. The authors declare no competing interests. Readers are welcome to comment on the online version of the paper. Publisher's note: Springer Nature remains neutral with regard to jurisdictional claims in published maps and institutional affiliations. Correspondence and requests for materials should be addressed to R.I.C. (ricitron@berkeley.edu).

Reviewer Information *Nature* thanks S. Bouley and M. Zuber for their contribution to the peer review of this work.

METHODS

Arabia shoreline (pre- or early-Tharsis formation). We assume deformation of the Arabia shoreline since its formation is due to global changes in topography resulting from Tharsis' formation (emplacement and loading) and the approximately 20° of Tharsis-induced TPW (Table 1).

The topographic response to TPW is given by the change in the flattening of the planet caused by the difference between the centrifugal potential at the initial and final rotation poles[10]. For a shoreline in place before TPW occurs, the deformation of the shoreline topography due to TPW[10] is:

$$\Delta T_{\mathrm{TPW}}(\theta, \varphi) = \frac{\omega^2 a^2}{3g}[P_{2,0}(\cos\gamma) - P_{2,0}(\cos\theta)][h_2 - (1 + k_2)] \quad (1)$$

where a is the mean planetary radius, ω is the rotation rate, g is the surface gravity, γ is the angular distance between a given current colatitude and longitude (θ, φ) and the palaeopole and h_2 and k_2 are the secular (fluid-limit) degree-2 Love numbers that depend on the density and elastic structure of Mars. The unnormalized degree-2 Legendre polynomial $P_{2,0}(\cos\eta) = \frac{1}{2}(3\cos^2\eta - 1)$.

The change in topography due to the emplacement of Tharsis and its associated loading is:

$$\Delta T_{\mathrm{Tharsis}}(\theta, \varphi) = S_{\mathrm{Tharsis}}(\theta, \varphi) - N_{\mathrm{Tharsis}}(\theta, \varphi) \quad (2)$$

where S_{Tharsis} and N_{Tharsis} are Tharsis' contribution to the shape and geoid of Mars, respectively. We use gravity and shape coefficients for Tharsis up to degree-5 from Matsuyama and Manga[14].

The current topography of the Arabia shoreline should therefore follow the deformation profile ΔT_{A}, given by:

$$\Delta T_{\mathrm{A}}(\theta, \varphi) = \Delta T_{\mathrm{TPW}}(\theta, \varphi) + \Delta T_{\mathrm{Tharsis}}(\theta, \varphi) + Z \quad (3)$$

where Z is a constant to adjust for the sea level at the time of the shoreline's emplacement. We minimize the least-squares misfit (σ_{rms}) between equation (3) and the shoreline elevation data for the Arabia contact examined in ref. 10 (data originally from ref. 7). We assume a fixed palaeopole (259.5° E, 71.1° N), corresponding to the fossil bulge[14]. We use an elastic lithosphere thickness $T_{\mathrm{e}} = 58$ km, the expected value at the time of Tharsis' emplacement[14], corresponding to $h_2 = 2.0$ and $k_2 = 1.1$[15].

We also test whether the Arabia shoreline can be explained by deformation due to only a certain percentage of Tharsis' emplacement and associated loading, by multiplying $\Delta T_{\mathrm{Tharsis}}$ in equation (3) by a factor C, corresponding to the percentage of Tharsis topography emplaced after shoreline formation (see Extended Data Fig. 3).

Deuteronilus shoreline (late-stage Tharsis formation). The Deuteronilus shoreline post-dates the initiation of Tharsis by >100 Myr, and therefore probably formed after a large portion of Tharsis was emplaced. The shoreline also probably post-dates most Tharsis-induced TPW, which should have occurred within a few million years of load emplacement[20]. Estimates of load-driven TPW on Mars suggest timescales less than 10 Myr[34–36], well within the required pre-Deuteronilus timescale. Although a fraction of the 20° of Tharsis-induced TPW may be due to relaxation of the lithosphere and occur on longer timescales[37], this should have a negligible effect given the small influence of TPW on shoreline deformation (Fig. 1a). Accordingly, we assume that deformation to the Deuteronilus shoreline since its formation is due to the topographic response of Mars to only the late stages of Tharsis' emplacement and associated loading. The current topography of the Deuteronilus shoreline should therefore follow the deformation profile ΔT_{D}, given by:

$$\Delta T_{\mathrm{D}}(\theta, \varphi) = C\Delta T_{\mathrm{Tharsis}}(\theta, \varphi) + Z \quad (4)$$

where $\Delta T_{\mathrm{Tharsis}}$ is deformation due to Tharsis (equation (2)), C is a constant representing how much of Tharsis formed after Deuteronilus was formed, and Z is a constant to adjust for sea level at the time of the shoreline's formation. We minimize the misfit between equation (4) and the Deuteronilus shoreline elevation data[18], to determine the optimal amount of Tharsis topography that should postdate the shoreline's formation.

Isidis shoreline (late-stage Tharsis formation). Because the Isidis shoreline is 100 Myr younger than Deuteronilus, we assume a similar deformation profile and compare equation (4) to the Isidis shoreline data[18]. We use the same value of C optimized for the Deuteronilus shoreline, but allow Z to vary, reflecting that sea level could change in the 100 Myr between the formation of the Deuteronilus contact and the Isidis contact, but deformation from Tharsis topography should not change substantially. Although C should be slightly less for Isidis, optimizing for C would result in an unrealistic $C = 0$ because deformation due to Tharsis along the Isidis shoreline results in a tilt that is opposite to the present tilt (Extended Data Fig. 4).

For the Isidis shoreline, our model predicts that deformation due to Tharsis would have tilted Isidis opposite to its present tilt (Extended Data Fig. 4). While this appears contradictory, the mismatch is possible if Isidis was tilted to its present orientation by loading of the Utopia basin. The Utopia basin has a large positive gravity anomaly[38,39], indicating about 18 km of excess fill[40]. Such a load would have caused elastic plate flexure and a peripheral bulge, which could have tilted the Isidis basin. Using a plate flexure model, McGowan and McGill[41] show that loading of Utopia could have tilted Isidis to an even greater extent than currently observed. Therefore, some amount of reverse tilting (as our model predicts) is possible. The timing of Utopia loading relative to the subsequent Tharsis deformation is irrelevant provided that Utopia loading also occurred after the Isidis shoreline formed. We expect loading of Utopia to occur after Isidis shoreline formation because a shrinking Martian ocean would evaporate from the Utopia basin last, depositing the non-volatile component of the ocean there. Additionally, if the ocean became cold and glacial during its decline[42], then receding glaciers may also have loaded Utopia with excess sediment. The deposits in the base of Utopia basin date to the early Amazonian (<3–3.46 Gyr ago)[43,44], after the emplacement of the Isidis shoreline. The eastern portion of Utopia also contains volcanic deposits from Elysium that date to the Amazonian[44], which could also contribute to loading. While loading from the ocean itself is expected to produce some plate flexure, it is not sufficient to explain the tilt of the Isidis basin (see Extended Data Fig. 5c), and water loading/unloading of Utopia is also insufficient to explain Isidis' tilt[41]. Therefore, deposition of material from a receding liquid, muddy or frozen ocean may explain the tilt of the Isidis basin, even if some reverse tilting is caused by deformation due to Tharsis.

Effect of elastic lithosphere thickness. The gravity and shape coefficients we use to subtract Tharsis topography are based on an assumed $T_{\mathrm{e}} = 58$ km, the expected value at the time of Tharsis loading[14]. However, the estimate of T_{e} yields a 90% confidence interval with a minimum and maximum of 26 km and 92 km, respectively[14]. A thinner or thicker T_{e} would alter the deformation due to Tharsis (and TPW) because the Love numbers used to compute Mars' deformation would change. To estimate the effect of $T_{\mathrm{e}} = 26$ km or 92 km on deformation due to Tharsis, we recompute Tharsis' gravity and shape coefficients following the method of ref. 14. Using a fixed Tharsis centre location (258.6° E, 9.8° N), Matsuyama and Manga[14] compute the degree-2 gravity coefficients of Tharsis using a minimization technique with four unconstrained model parameters (T_{e}, non-dimensional Tharsis load Q, palaeopole colatitude θ_{R} and palaeopole longitude φ_{R}), where the palaeopole corresponds to the axis of rotation when the fossil (remnant) bulge was formed. This results in probability density functions for each unconstrained parameter, with the weighted averages (expected values) used to compute the gravity and shape coefficients. We redo this analysis, as described in section 5 of ref. 14, but with T_{e} treated as a constrained parameter. This allows us to estimate the expected values of Q, θ_{R} and φ_{R} for a given value of T_{e}. We find that for $T_{\mathrm{e}} = 26$ km, $\overline{Q} = 3.95$, $\overline{\theta}_{\mathrm{R}} = 17.9°$, and $\overline{\varphi}_{\mathrm{R}} = 259.1°$. For $T_{\mathrm{e}} = 92$ km, $\overline{Q} = 1.57$, $\overline{\theta}_{\mathrm{R}} = 14.2°$, and $\overline{\varphi}_{\mathrm{R}} = 259.3°$. Tharsis' degree-2 gravity coefficients are recomputed using these values. The degree-3 to -5 gravity coefficients of Tharsis are computed from minimization against the observed degree-3 to -5 gravity coefficients, and are therefore not dependent on T_{e}. Shape coefficients for Tharsis are computed up to degree 5 following section 7 of ref. 14. We compute the load Love numbers using the ALMA code[45], with a five-layer model as described in ref. 14.

We construct new best-fit deformation profiles for $T_{\mathrm{e}} = 26$ km and 92 km, but with the corresponding Tharsis gravity and shape coefficients that we computed for each T_{e}. The best-fit profiles for $T_{\mathrm{e}} = 26$ km and 92 km are compared with the nominal $T_{\mathrm{e}} = 58$ km profiles in Extended Data Fig. 3. All best-fit profiles are relatively similar, showing that changes in T_{e} do not have much effect on our conclusions.

Effect of plate flexure. Although Perron *et al.*[10] found that plate flexure due to loading of the ocean basin should not substantially affect the shoreline elevations, their analysis was for $T_{\mathrm{e}} = 200$ km, whereas we use $T_{\mathrm{e}} = 58$ km. The ocean basin resulting from our analysis also has less volume and a different shape, because we subtract Tharsis topography, which has a negative component in much of the Borealis basin. To compute plate flexure due to ocean loading, we expand the surface density of the ocean load in spherical harmonics and compute the associated displacement using the method described in ref. 46. For the Arabia ocean, the ocean load is computed by subtracting the pre-Tharsis topography of Mars from the best-fit Arabia ocean elevation ($Z = -2.3$ km). The pre-Tharsis Martian topography is computed by subtracting the deformation due to Tharsis and TPW, equations (2) and (1), from Mars' current topography (0.25° per pixel gridded MOLA data[21]). For the ocean level corresponding to the Deuteronilus and Isidis shorelines, only 17% of deformation due to Tharsis was subtracted from Mars' current topography, and the ocean elevation Z was set to −3.68 km and −3.95 km, respectively. We use a Young's modulus of 70 GPa, Poisson ratio of 0.25, and an assumed value of $T_{\mathrm{e}} = 58$ km. The loaded shoreline topography is compared to the

unloaded topography in Extended Data Fig. 5. We compute a maximum magnitude of deflection of 134 m, 84 m and 57 m, for the Arabia, Deuteronilus and Isidis shorelines, respectively. The mean magnitude of deflection is 35 m for the Arabia shoreline and 17 m for the Deuteronilus and Isidis shorelines. Deformation of the shorelines due to unloading of the ocean basin is negligible.

Data availability. The data that supports the findings of this study are available on request from the corresponding author. Gravity and shape coefficients for Tharsis are included in the Supplementary Information. Shoreline data should be requested from the respective sources.

34. Harada, Y. Long-term polar motion on a quasi-fluid planetary body with an elastic lithosphere: semi-analytic solutions of the time-dependent equation. *Icarus* **220,** 449–465 (2012).
35. Chan, N.-H. *et al.* Time-dependent rotational stability of dynamic planets with elastic lithospheres. *J. Geophys. Res. Planets* **119,** 169–188 (2014).
36. Hu, H., van der Wal, W. & Vermeersen, L. L. A. A full-Maxwell approach for large angle polar wander of viscoelastic bodies. *J. Geophys. Res. Planets* **122,** 2745–2764 (2017).
37. Moore, K. M., Chan, N.-H., Daradich, A. & Mitrovica, J. X. Time-dependent rotational stability of dynamic planets with viscoelastic lithospheres. *Icarus* **289,** 34–41 (2017).
38. Sjogren, W. L. Mars gravity: high-resolution results from Viking Orbiter 2. *Science* **203,** 1006–1010 (1979).
39. Zuber, M. T. *et al.* Internal structure and early thermal evolution of Mars from Mars Global Surveyor topography and gravity. *Science* **287,** 1788–1793 (2000).
40. Searls, M. L., Banerdt, W. B. & Phillips, R. J. Utopia and Hellas basins, Mars: twins separated at birth. *J. Geophys. Res. Planets* **111,** E08005 (2006).
41. McGowan, E. M. & McGill, G. E. Anomalous tilt of Isidis Planitia, Mars. *Geophys. Res. Lett.* **33,** L08S06 (2006).
42. Fairén, A. G. A cold and wet Mars. *Icarus* **208,** 165–175 (2010).
43. Werner, S. C. & Tanaka, K. L. Redefinition of the crater-density and absolute-age boundaries for the chronostratigraphic system of Mars. *Icarus* **215,** 603–607 (2011).
44. Tanaka, K. L., Robbins, S. J., Fortezzo, C. M., Skinner, J. A. & Hare, T. M. The digital global geologic map of Mars: chronostratigraphic ages, topographic and crater morphologic characteristics, and updated resurfacing history. *Planet. Space Sci.* **95,** 11–24 (2014).
45. Spada, G. ALMA, a Fortran program for computing the viscoelastic Love numbers of a spherically symmetric planet. *Comput. Geosci.* **34,** 667–687 (2008).
46. Arkani-Hamed, J. The lunar mascons revisited. *J. Geophys. Res. Planets* **103,** 3709–3739 (1998).

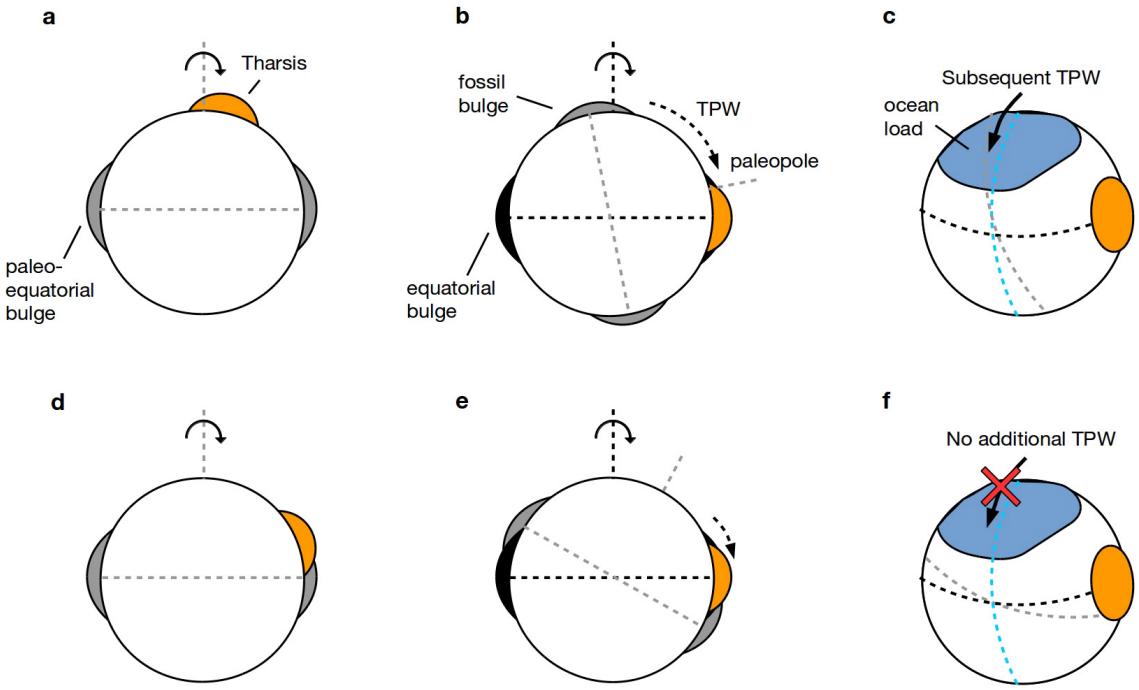

Extended Data Figure 1 | Illustration of the feasibility of post-Tharsis TPW depending on the location of Tharsis' formation. a–c, Tharsis (orange zone) forms far from the palaeo-equator (**a**), causing large-scale TPW as the planet reorients so Tharsis is at the equator (**b**). After the reorientation, the fossil bulge is far from the current equatorial bulge, making the rotation pole sufficiently unstable to allow for ocean loading (blue zone) to cause subsequent TPW along an arc 90° from Tharsis (**c**, blue dashed line)[10]. **d–f,** Alternatively, Tharsis forms near the palaeo-equator (**d**), causing limited (approximately 20°) TPW (**e**). The position of the fossil bulge near the equator stabilizes the planet against subsequent TPW caused by oceans and other surface loads (**f,** see supplementary figure 1 of ref. 10). Formation of Tharsis near the equator is supported by refs 14 and 15.

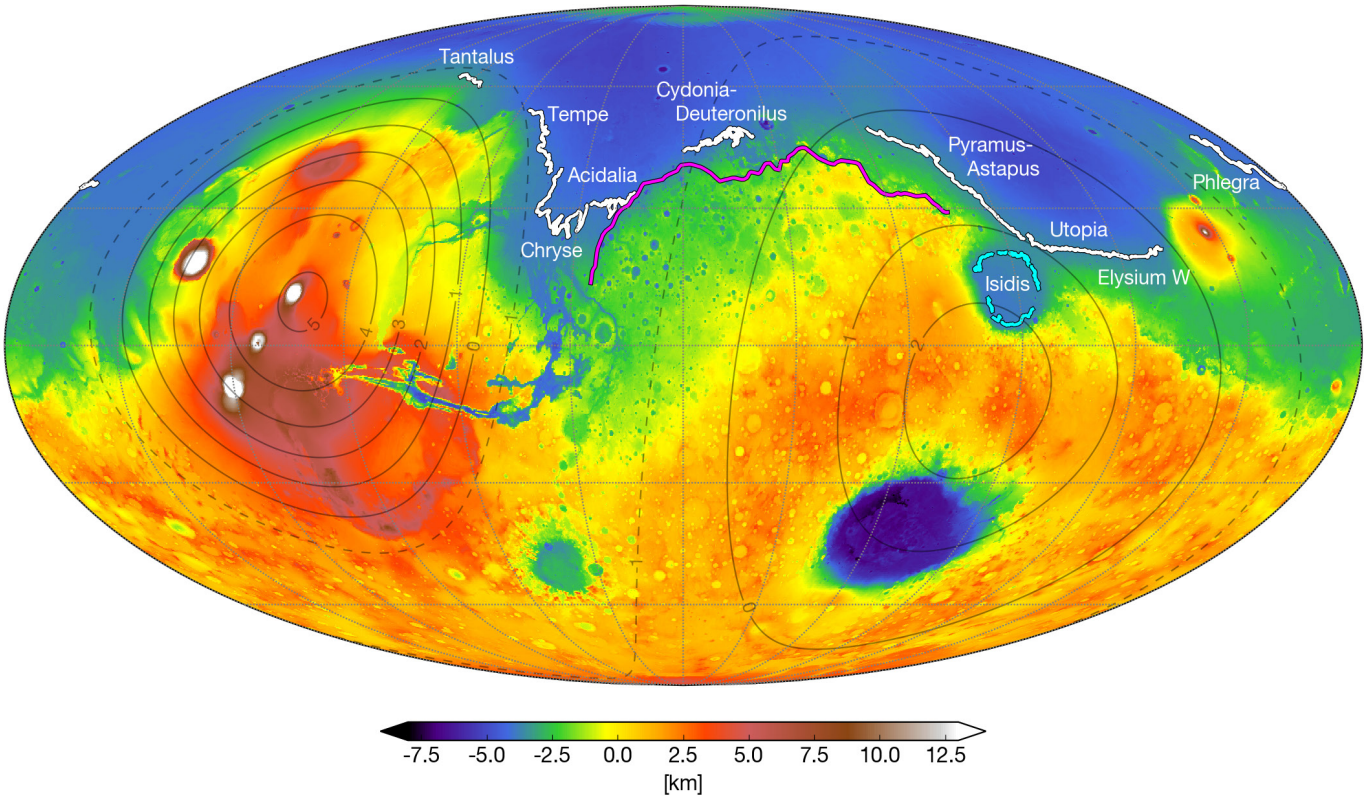

Extended Data Figure 2 | Map of shoreline locations, MOLA topography, and Tharsis deformation. Arabia (magenta) shoreline data are from ref. 10 (data originally from ref. 7). Deuteronilus (white) and Isidis (cyan) shoreline data and regional names are from ref. 18. The contribution of Tharsis to Mars' topography up to degree-5 (equation (2)) is displayed as 1-km dark grey contours (dashed contours are negative).

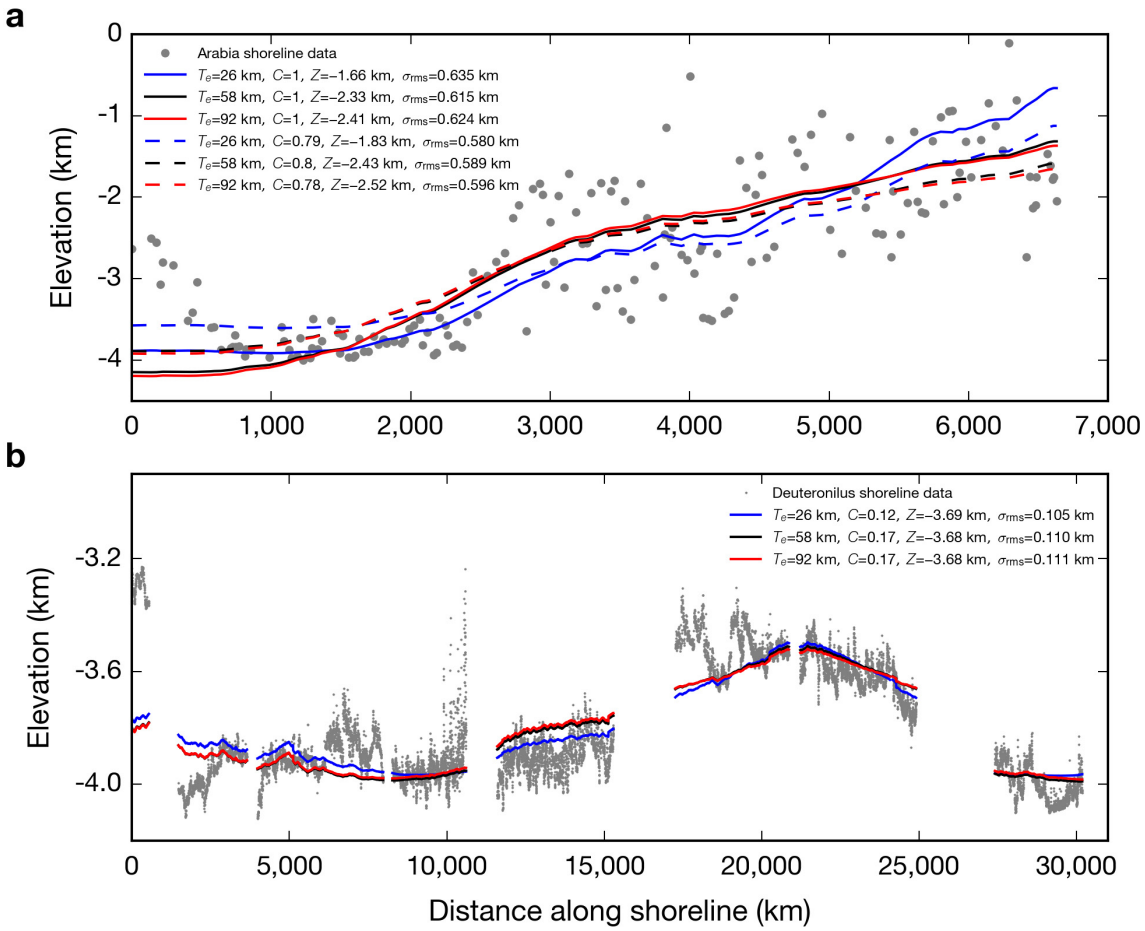

Extended Data Figure 3 | Effect of elastic lithosphere thickness on deformation due to Tharsis. a, Current Arabia shoreline topography compared to displacement due to TPW and Tharsis deformation (equation (3)). Tharsis gravity and shape coefficients are computed separately for $T_e = 26$ km, 58 km and 92 km (see Methods), which each yield a corresponding best-fit offset Z and error σ_{rms}. Dashed lines show the best fit when the percentage of Tharsis topography added after shoreline formation was allowed to vary by a factor C. Solid lines assume 100% percent of Tharsis topography was emplaced after shoreline formation ($C = 1$). **b**, Deuteronilus shoreline topography compared to the best-fit displacement due to Tharsis loading (equation (4)) for $T_e = 26$ km, 58 km and 92 km.

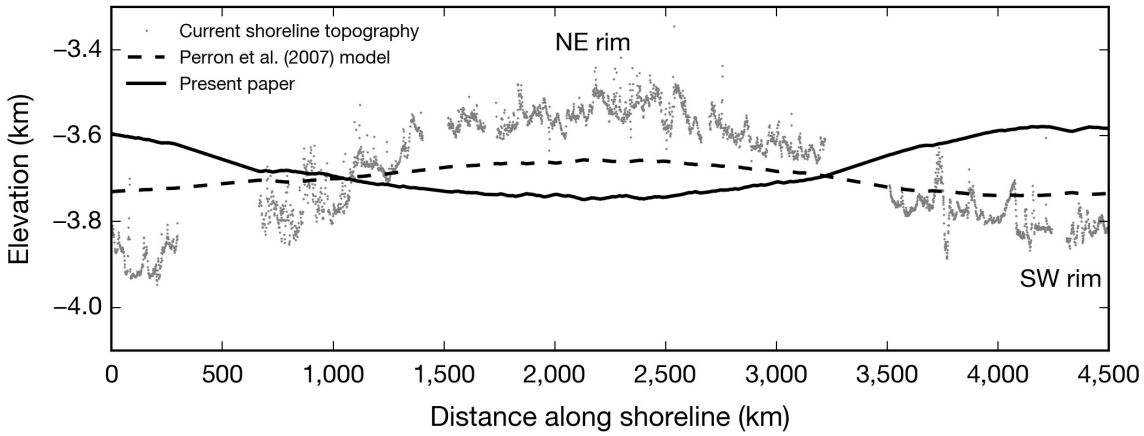

Extended Data Figure 4 | Comparison of Isidis shoreline topography to shoreline deformation models. Current Isidis shoreline topography (elevation data from ref. 18) compared to the Perron *et al.*[10] model for $T_e = 200$ km and our model of deformation due to partial Tharsis emplacement ($0.17\Delta T_{\text{Tharsis}} - 3.95$ km). The topography of the Isidis shoreline can be explained by subsequent loading of the Utopia basin (see Methods). The starting point for the shoreline is (82.32° E, 7.36° N), near the southwest (SW) rim, with shoreline data proceeding clockwise through the northeast (NE) rim.

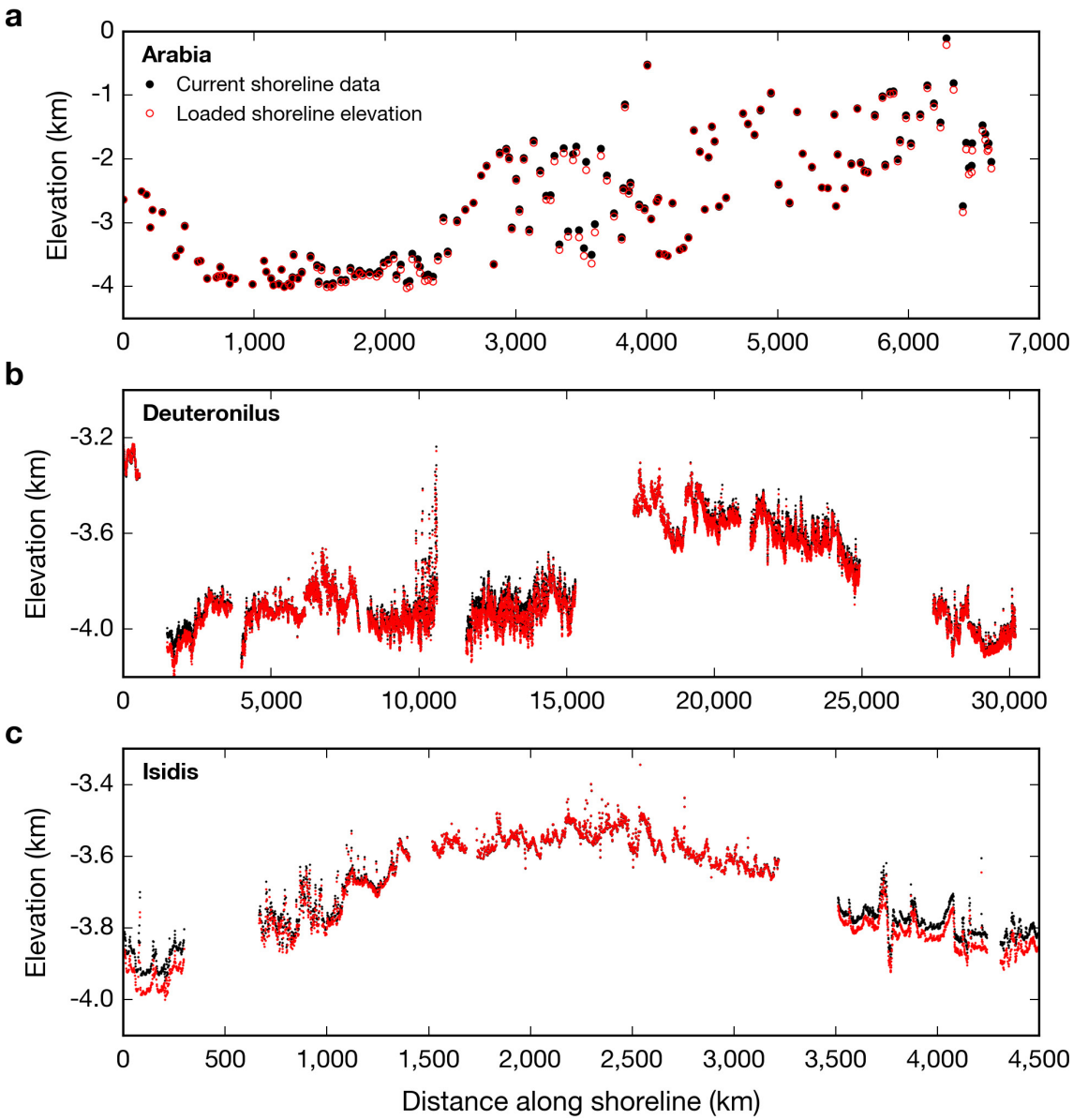

Extended Data Figure 5 | Effect of plate flexure due to ocean loading on shoreline topography. Current shoreline elevations are plotted against displaced elevations for the Arabia shoreline (**a**), the Deuteronilus shoreline (**b**) and the Isidis shoreline (**c**).